Desalination and Water Treatment
www.deswater.com

doi: 10.1080/19443994.2013.815689

52 (2014) 6088–6095
September

Taylor & Francis
Taylor & Francis Group

Adsorption of cationic dye using a low-cost biowaste adsorbent: equilibrium, kinetic, and thermodynamic study

R.R. Krishni[a], K.Y. Foo[b], B.H. Hameed[a,*]

[a]*School of Chemical Engineering, Engineering Campus, Universiti Sains Malaysia, Nibong Tebal, Penang 14300, Malaysia*
Tel. +604 5996422; Fax: +604 5941013; email: chbassim@eng.usm.my
[b]*Environment and Occupational Health Programme, School of Health Sciences, Health Campus, Universiti Sains Malaysia, Kubang Kerian, Kelantan 16150, Malaysia*

Received 2 August 2012; Accepted 23 May 2013

ABSTRACT

In this study, papaya stem, an agricultural biomass abundantly available in Malaysia, was utilized as low-cost adsorbent for removing methylene blue from the aqueous solution. The textural and functional characterization was evaluated using the scanning electron microscopy and Fourier transform infrared analysis. The adsorption data were simulated using the nonlinear Langmuir, Freundlich and Temkin isotherm models. Kinetic modeling and adsorption mechanism were fitted to the pseudo-first-order, pseudo-second-order, and intraparticle diffusion models. Thermodynamic parameters, enthalpy, entropy, and Gibb free energy changes were established. Equilibrium data were best described by the Langmuir isotherm equation, with a monolayer adsorption capacity of 260.95 mg/g. The results supported the potential use of papaya stem as an efficient adsorbent for the treatment of cationic dye.

Keywords: Adsorption; Equilibrium; Isotherm; Kinetic; Methylene blue; Papaya stem

1. Introduction

Papaya (*Carica papaya*) is a plant species belongs to the genus *Carica* and family of Caricaceae [1]. It is a single-stem plant, growing from 5 to 10 m tall, with spirally arranged leaves confined to the top of the trunk [2]. Papaya tree is planted for its fruits. The ripe fruit is primarily eaten fresh, while the unripe fruit can be eaten cooked, usually in curries, salads, and stews. The black seeds, which have a sharp, spicy taste, are grounded and used as a substitute for black pepper [3]. However, the papaya stem, which has low-economic use, is usually burnt as fuel or discarded as waste.

Over the years, adsorption is recognized as a promising and most widely used technique in the wastewater treatment processes [4]. For this purpose, activated carbon, an adsorbent with its large porous surface area, controllable pore structure, and low acid/base reactivity [5], has been proven to be effective for removing a wide variety of pollutants, even from the gaseous environment [6]. The biggest barrier of its application by the industries is the cost-prohibitive adsorbent and difficulties associated with regeneration [7]. This has exerted to a growing exploitation to investigate the suitability of renewable and low cost materials as alternative adsorbents in the water pollution control [8]. This study was carried out

*Corresponding author.

intended to examine the adsorption potential of papaya stem as a low-cost adsorbent for removing methylene blue dye from the aqueous solutions. The morphological and functional characterization of the prepared adsorbent was performed. Moreover, the effect of initial dye concentration, contact time, solution pH, adsorption isotherm, kinetics, thermodynamics, and mechanism are elucidated.

2. Materials and methods

2.1. Adsorbate

Methylene blue (MB), a basic dye with the molecular structure $C_{16}H_{18}N_3ClS$, supplied by Sigma-Aldrich (M) Sdn. Bhd, Malaysia was chosen as the model adsorbate in this study. The standard stock solution was prepared by dissolving accurately weight dye in distilled water to a concentration of 1,000 mg/L. The experimental solutions were prepared by diluting the stock solution in accurate proportions to the desired concentrations.

2.2. Preparation and characterization of adsorbent

Papaya stems required in this work were collected from a local papaya plantation area. The precursor was cleaned, cut into small pieces (1–2 cm), grounded and screened to a particle fraction of 500 μm. The sample was then washed repeatedly with hot distilled water, dried at 70°C, and stored in plastic containers. The textural structure of the adsorbent before and after the adsorption of dye was analyzed using the scanning electron microscopy (SEM). The surface functional groups were detected by Fourier transform infrared (FTIR) spectroscope (FTIR-2000, PerkinElmer) from the scanning range of 4,000–400 cm^{-1}.

2.3. Batch equilibrium studies

The batch equilibrium studies were conducted in a set of 250-mL Erlenmeyer flasks containing 0.30 g of adsorbent and 200 mL of MB solutions within the concentrations of 50–300 mg/L. The mixture was agitated at 120 rpm and 30°C for 360 min until the equilibrium was reached. All samples were filtered using a syringe filter (Whatman 0.45 μm) prior to analysis to minimize interference of adsorbent fines with the analysis. The concentration of MB dye solution was determined using a double-beam UV–vis spectrophotometer (UV-1601 Shimadzu, Japan) at 668 nm. Each experiment was duplicated under identical conditions. The MB uptake at equilibrium, q_e (mg/g), was calculated by:

$$q_e = \frac{(C_0 - C_e)V}{W} \quad (1)$$

where C_0 and C_e (mg/L) are the liquid-phase concentrations of dye at initial and equilibrium, respectively. V is the volume of solution (L), and W is the mass of adsorbent used (g). The effect of solution pH on the adsorptive uptake of MB was examined by varying the solution pH from pH 2 to 10, at the fixed MB concentration of 200 mg/L, adsorbent dosage of 0.15 g/100 mL and adsorption temperature of 30°C. The initial pH of the dye solution was adjusted by addition of 0.10 M solution of HCl or NaOH. The procedure of adsorption kinetic was identical to the batch equilibrium studies, where the aqueous samples were withdrawn at different time intervals and the concentrations of MB were similarly measured. The amount of adsorption at time t, q_t (mg/g), was calculated by:

$$q_t = \frac{(C_0 - C_t)V}{W} \quad (2)$$

where C_t (mg/L) is the liquid-phase concentrations of dye at time t (min).

3. Results and discussion

3.1. Characterization of the prepared adsorbent

The scanning electron micrographs (SEM) of the papaya stem derived adsorbent before and after the adsorption of MB is depicted in Fig. 1. From Fig. 1, it can be clearly seen that the adsorbent surface showed an even and heterogeneous structure (Fig. 1(a)), indicating good possibility for the dyes to be trapped and adsorbed. However, the surface of the dye-loaded adsorbent displayed a rougher texture, covered with the adsorbed MB dye molecules (Fig. 1(b)).

The representative FTIR spectrum of the papaya stem derived adsorbents before and after the adsorption of MB is shown in Table 1. The transmittance at 3,427/3,421, 2,920/2,919, 1,735 and 1,624/1,621 cm^{-1} are corresponded to the hydroxyl (–OH), alkyl (–CH_2), carbonyl (C=O) and C=C groups of alkene. The sharps peaks at 1,508/1,491, 1,423, 1,394, 1,375, 1,356, and 1,318/1,317 cm^{-1} are ascribed to the presence of NH_3^+, C–O dimmers, H–C=O bends aliphatic aldehydes, –CH_3, NO_2 aromatic nitro compounds and –CH_3 groups of benzene. The signals at 1,253/1,251, 1,157/1,152, 1,101 and 1,058/1,055 cm^{-1} are associated with the C–O–C, C–N, –C–NH_3 primary aliphatic amines and S=O alkyl sulfoxides derivatives and intensive peaks at 1,035, 895/886, 781 and 667 cm^{-1} are related to the P–O–C, out-of-plane CH, C–Cl and

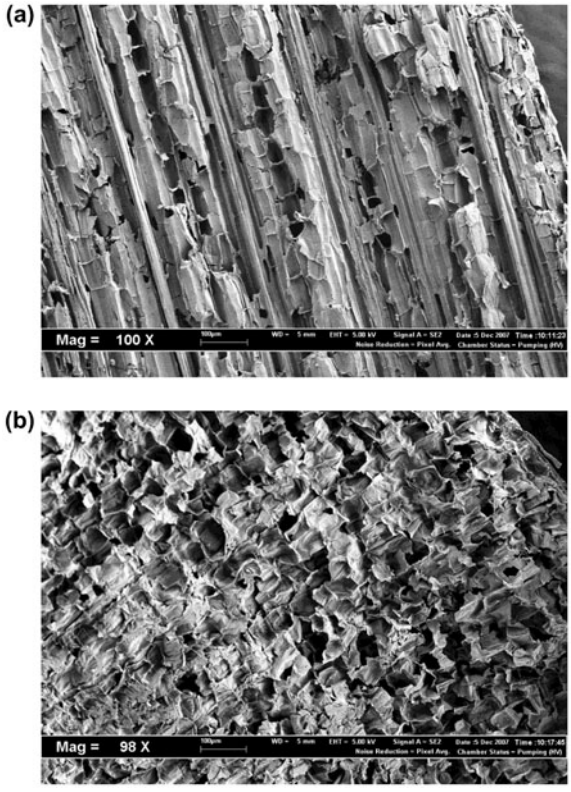

Fig. 1. SEM micrographs (100 X) for the papaya stem-derived adsorbent (a) before and (b) after the adsorption of MB.

C–O–H functionalities. Meanwhile, the surface chemistry of the papaya stem derived adsorbent revealed some shift, disappear and new peaks after the adsorption of MB, indicating possible involvement of the functional groups during the adsorption process.

3.2. Batch adsorption studies

The effects of contact time and initial dye concentration on the adsorptive uptake of MB is displayed Fig. 2. The adsorptive uptake of MB increased with prolonging the contact time. The plots can be divided into three distinct regions: rapid adsorption during the early stage, gradual adsorption till the equilibrium state and a plateau. At this point, the dye desorbing from the adsorbent is in a state of dynamic equilibrium with the amount of dye being adsorbed onto the adsorbent. The time required to attain this state of equilibrium is termed as equilibrium time [9]. This phenomenon is attributed to the reduction of immediate solute adsorption due to the lack available open sites for dye adsorption, which in turn supported film diffusion [10]. Similar behavior was observed in the adsorption of MB onto Shaddock peel and clay particles [11,12].

Initial concentration provides a driving force to overcome mass transfer resistances of dye molecules between aqueous solution and the solid medium [13]. In the present study, the adsorption equilibrium of MB, q_e increased from 34.90 to 163.15 mg/g with an increase in initial concentration from 50 to 300 mg/L. The time profile of dye uptake is a single, smooth and continuous curve leading to saturation, suggesting possible monolayer coverage of dye onto the surface of papaya stem [14].

Solution pH affects adsorption by regulating the dissociation of adsorbents surface charge as well as degree of ionization of adsorbates present in the solution (Fig. 3). It is evident from Fig. 3 that increasing solution pH from 2 to 10 indicated an increasing q_e from 46.78 to 124.60 mg/g, with a significant enhancement as the solution pH increased from 2 to 4. Lower adsorption at strong acidic pH is due to the presence of H_3O^+ ions competing with dye cations for the adsorption sites. In the basic medium, the number of negatively charged sites increased, and the formation of electric double layer changes its polarity, which favors the adsorption of MB cations [15]. The result is in good agreements with the previous studies [16,17].

3.3. Adsorption isotherm

In the endeavor to explore novel adsorbents in accessing an ideal adsorption system, it is essential to establish the most appropriate equilibrium correlation, which is indispensable for reliable prediction of adsorption parameters for varied experimental conditions [18]. Due to the inherent bias resulting from linearization, alternative isotherm parameter sets were determined by non-linear regression. The equilibrium data were modeled using the Langmuir [19], Freundlich [20] and Temkin [21] isotherm models.

Langmuir isotherm [19] assumes monolayer adsorption with adsorption can only occur at a finite number of localized sites that are identical and equivalent. Langmuir isotherm is defined as follows:

$$q_e = \frac{Q_0 K_L C_e}{1 + K_L C_e} \tag{3}$$

where Q_0 (mg/g) and K_L (L/g) are Langmuir constants related to adsorption capacity and energy of adsorption.

Freundlich isotherm [20] is a relationship describing the nonideal and reversible adsorption. The model assumes multilayer adsorption, with nonuniform

Table 1
Comparison of Fourier transform infrared spectroscopy (FTIR) of the papaya stem-derived adsorbent before and after the adsorption of MB

IR peak	Frequency (cm^{-1})		Assignation
	Before adsorption	After adsorption	
1	3,421	3,427	Bonded –OH groups
2	2,920	2,919	Two bands for $–CH_2–$ groups
3	1,735	1,735	C=O stretching
4	1,624	1,621	C=C stretching
5	1,508	1,491	NH_3^+ deformation
6	1,423	–	In-plane –OH bending and C–O stretch of dimmers
7	–	1,394	H–C=O bends aliphatic aldehydes
8	1,375	–	CH_3 deformation
9	–	1,356	$–NO_2$ aromatic nitro compounds
10	1,318	1,317	$–CH_3$ attached to a benzene ring
11	1,253	1,251	C–O–C stretch
12	1,157	1,152	C–N stretching
13	–	1,101	$–C–NH_3$ primary aliphatic amines
14	1,055	1,058	S=O alkyl sulfoxides
15	–	1,035	P–O–C strongest band highest frequencies for aliphatic amines
16	895	886	CH out-of-plane deformation
17	781	781	C–Cl stretch
18	667	667	C–O–H twist broad

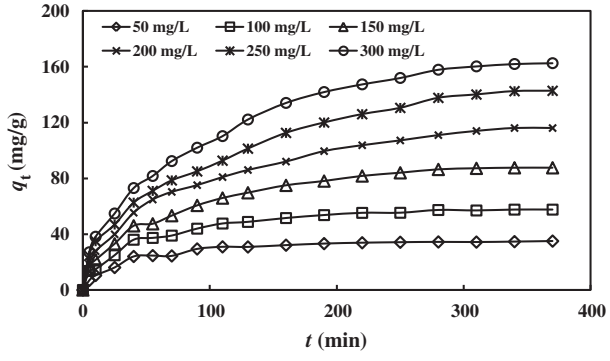

Fig. 2. Effects of initial concentration and contact time on the adsorptive uptake of MB onto the papaya stem-derived adsorbent (conditions: $W = 0.30\,g/200\,mL$; temperature = 30°C).

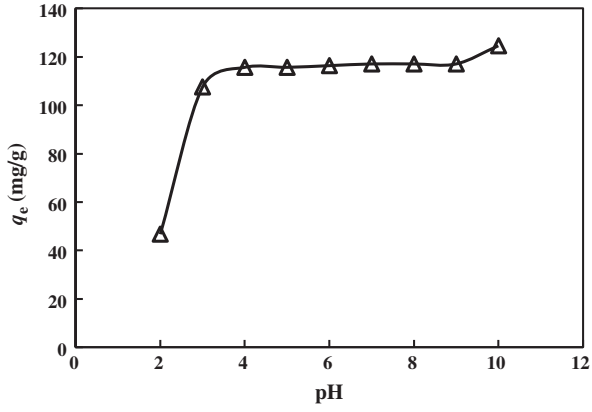

Fig. 3. Effect of solution pH on the adsorption of MB onto the papaya stem-derived adsorbent (conditions: $W = 0.30\,g/200\,mL$; $C_0 = 200\,mg/L$; temperature 30°C).

distribution of adsorption heat and affinities over the heterogeneous surface.

$$q_e = K_F C_e^{1/n} \quad (4)$$

where K_F (mg/g) $(L/mg)^{1/n}$ and $1/n$ are the Freundlich adsorption constant and a measure of adsorption intensity.

Temkin isotherm [21] assumes that the heat of adsorption of all molecules in the layer would decrease linearly rather than logarithmically with surface coverage. Temkin isotherm has been used in the form of:

$$q_e = B \ln(A C_e) \quad (5)$$

where $B = RT/b$, and b (J/mol), A (L/g), R (8.314 J/mol K) and T (K) are the Temkin constant related to heat of sorption, equilibrium binding constant, gas constant and absolute temperature.

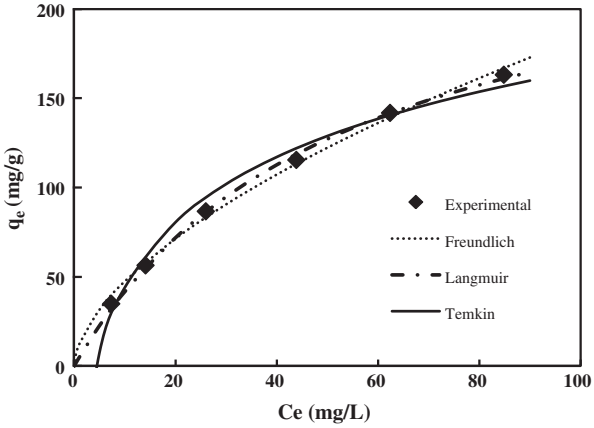

Fig. 4. Plots of Langmuir, Freundlich and Temkin isotherm models for the adsorption of MB onto the papaya stem-derived adsorbent at 30°C.

Fig. 4 and Table 2 show the plots of isotherm models couple with the isotherm constants. The equilibrium data agreed satisfactory with the Langmuir isotherm model, with the R^2 higher than 0.99 at 30°C. The correlation coefficient, R^2 fitted with Freundlich and Temkin isotherm model was found much lower than the Langmuir isotherm model. The result suggested that the adsorption process is monolayer with each molecule poses equal enthalpies and activation energy. The findings also demonstrated no interaction and transmigration of dyes in the plane of the neighboring surface. A comparison of the monolayer adsorption capacities of MB onto various adsorbents [17,22–28] is listed in Table 3. The adsorbent prepared in this work showed relatively high adsorption capacity for MB of 260.95 mg/g, as compared to some previous works as reported in the literature.

3.4. Adsorption kinetics

Adsorption kinetics describes the solute uptake, which governs the mechanism of the adsorption process [29]. Lagergren [30] proposed pseudo-first-order kinetic model in the form of:

$$\log\left(\frac{q_e}{q_e - q_t}\right) = \frac{k_1}{2.303}t \tag{6}$$

where k_1 is the adsorption rate constant (1/min). Pseudo-second-order equation [31] predicts the behavior over the whole range of adsorption, with chemisorption being the rate controlling step. The pseudo-second-order kinetic model is expressed as:

$$\frac{t}{q_t} = \frac{1}{k_2 q_e^2} + \frac{1}{q_e}t \tag{7}$$

where k_2 (g/mg min) is the pseudo-second-order kinetic rate constant. The values of k_1 were obtained from the slopes of the linear plots of log $[q_e/(q_e - q_t)]$ vs. t, as shown in Fig. 5(a). The linear plot of t/q_t vs. t gave $1/q_e$ as the slope and $1/k_2\ q_e^2$ as the intercept (Fig. 5(b)). The corresponding results are tabulated in Table 4. The result revealed good agreement with the pseudo-second-order kinetic model, with the correlation coefficients greater than 0.97 for all MB concentrations. Moreover, the experimental q_e values agreed satisfactory with the calculated q_e values obtained

Table 2
Langmuir, Freundlich and Temkin isotherm constants for the adsorption of MB onto papaya stem-derived adsorbent

Isotherm	Constants
Langmuir isotherm model	
Q_0 (mg/g)	260.95
K_L (L/mg)	0.019
R^2	0.998
Freundlich isotherm model	
K_F (mg/g) (L/mg)$^{1/n}$	12.24
n	1.70
R^2	0.993
Temkin isotherm model	
A (L/g)	0.23
B	52.76
R^2	0.977

Table 3
Comparison of adsorption capacities of various adsorbents for MB

Adsorbent	Q_0 (mg/g)	Temperature (°C)	Reference
Papaya stem	260.95	30	This study
Cottonseed hull	185.22	30	[17]
Natural zeolite	19.94	25	[22]
Natural palygorskite clay	48.39	30	[23]
Fly ash	10.20	30	[24]
Graphene	153.85		[25]
Rice straw activated carbon	129.50	25	[26]
Durian peel activated carbon	284.00	30	[27]
Pine wood activated carbon	200.00	30	[28]

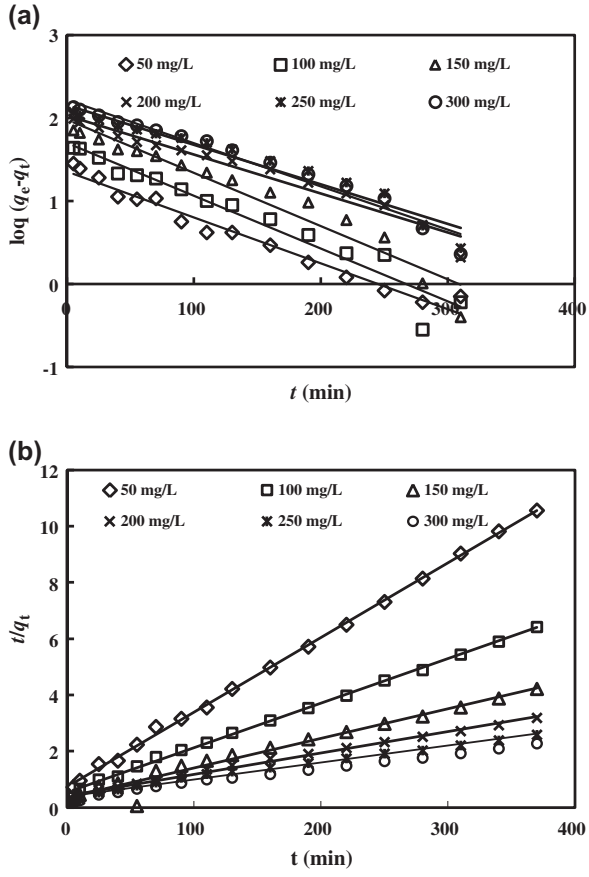

Fig. 5. Plots of (a) pseudo-first-order and (b) pseudo-second-order kinetic models for the adsorption of MB onto papaya stem-derived adsorbent at 30°C.

theoretically. This showed that the adsorption of MB onto the papaya stem-based adsorbent followed pseudo-second-order equation, which suggested that chemisorption, which involved valency forces through electrons sharing between MB and the adsorbent is the rate-limiting step.

3.5. Adsorption thermodynamics and mechanism

Adsorption thermodynamic is an important tool elucidating the adsorption behavior of an isolated system [32]. In this work, the effect of solution temperature on the adsorption process was conducted at the adsorption temperature of 30, 40, and 50°C. The values of enthalpy change (ΔH), Gibbs free energy change (ΔG), and entropy change (ΔS) were computed following the equations:

$$\ln K_L = \frac{\Delta S}{R} - \frac{\Delta H}{RT} \quad (8)$$

$$\Delta G = -RT \ln K_L \quad (9)$$

where R (8.314 J/mol K) is the universal gas constant, T (K) is the absolute solution temperature and K_L (L/mg) is the Langmuir isotherm constant.

Positive ΔS (91.67 J/mol K) indicates the affinity of papaya stem and increasing randomness at the solid/solution interface during the adsorption process. Negative ΔH (−17.99 kJ/mol) illustrates exothermic nature of the adsorption process, where increasing temperature showed a gradually decrease in adsorptive uptake, due to the weakening of adsorptive forces between the active sites and the dye species, and between the adjacent dye molecules on the adsorbed phase. Positive ΔG reflects nonspontaneous nature of the adsorption process at the studied temperatures. The value of ΔG was 9.97 kJ/mol at 30°C, and this ΔG value turned higher at higher operating temperature of 40 (10.30 kJ/mol) and 50 (11.83 kJ/mol) °C. This shows that the reaction rate decreased with increasing the operating temperature. The results were consistent with the earlier findings, where the adsorption of MB onto papaya stem was exothermic in nature. Similar trend was reported for the adsorption of Acid Orange dye onto *Paulownia tomentosa* Steud. leaf powder [33].

Table 4
Kinetic models parameters for the adsorption of MB onto papaya stem-derived adsorbent at different initial MB concentrations

C_0 (mg/L)	Pseudo-first-order kinetic model				Pseudo-second-order kinetic model		
	$q_{e,\,exp}$ (mg/g)	$q_{e,\,cal}$ (mg/g)	k_1 (1/min)	R^2	$q_{e,\,cal}$ (mg/g)	k_2 (g/mg min)	R^2
50	35.03	25.02	0.014	0.996	38.02	0.0009	0.976
100	57.60	44.44	0.013	0.993	62.11	0.0005	0.991
150	87.60	72.74	0.011	0.888	87.72	0.0004	0.996
200	116.09	93.67	0.009	0.985	119.05	0.0002	0.991
250	142.76	119.95	0.009	0.968	144.93	0.0001	0.994
300	162.60	141.12	0.001	0.972	175.44	0.0001	0.996

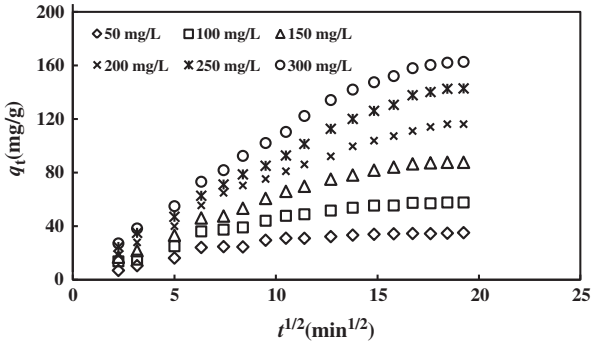

Fig. 6. Plots of intraparticle diffusion model for different initial MB concentrations at 30°C.

The adsorption mechanism was further analyzed using the intraparticle diffusion model, an empirical model [34] describing the relationship for the adsorptive uptake of MB proportional to $t^{1/2}$:

$$q_t = k_{id} t^{1/2} + C \quad (10)$$

where C is the intercept and k_{id} is the intraparticle diffusion rate constant (mg/g min$^{0.5}$).

The intraparticle diffusion plots for the adsorption of MB onto the papaya stem-derived adsorbent of the concentrations of 50–300 mg/L are presented in Fig. 6. The first region is the instantaneous adsorption, representing the mass transfer of adsorbate molecules from bulk solution to the adsorbent surface. The second region is the gradual adsorption stage. The third region is the final equilibrium stage, where intraparticle diffusion started to slow down due to the extremely low adsorbate concentrations left in the solutions [35].

Refer to the intraparticle diffusion plot (Fig. 6), the linear lines of the second and third stages did not pass through the origin, due to the difference in the mass transfer rate in the initial and final stages of adsorption. Besides the linear curves did not pass through the origin, and the points were scattered around the plots. This implied that intraparticle diffusion was not the only rate limiting mechanism in the adsorption process. The deviation exhibits the presence of multilinearity, indicating the transportation of adsorbate from solution phase to the surface of adsorbent is controlled by a combination of more than one step (film or external diffusion, pore diffusion, surface diffusion and adsorption onto the pore surface) [36].

4. Conclusion

The present investigation revealed the viability of papaya stem-developed adsorbent for removing cationic dye from aqueous solutions over a wide range of concentrations. Adsorption data were favorably described by the Langmuir isotherm model, with a monolayer adsorption capacity of 260.95 mg/g. The kinetic data agreed satisfactory with the pseudo-second-order kinetic model, suggesting a chemisorption process.

References

[1] D. Gonsalves, Control of papaya ringspot virus in papaya: A case study, Annu. Rev. Phytopathol. 36 (1998) 415–437.
[2] J. Morton, Papaya, in: J.F. Morton (Ed.), Fruits of Warm Climates, Creative Resource Systems, Miami, FL, 1987, pp. 336–346.
[3] N.K. Lohiya, B. Manivannan, P.K. Mishra, N. Pathak, S. Sriram, S.S. Bhande, S. Panneerdoss, Chloroform extract of *Carica papaya* seeds induces long-term reversible azoospermia in langur monkey, Asian J. Andrology 4 (2002) 17–26.
[4] C.S. Ozdemir, Modeling of tartrazine adsorption onto activated carbon fiber in a continuous fixed-bed reactor, Desalin. Water Treat. 46 (2012) 234–243.
[5] A.O. Alade, O.S. Amuda, A.O. Ibrahim, Isothermal studies of adsorption of acenaphthene from aqueous solution onto activated carbon produced from rice (Oryza sativa) husk, Desalin. Water Treat. 46 (2012) 87–95.
[6] N. Bouchemala, Y. Azoudj, Z. Merzougu, F. Addoun, Adsorption modeling of Orange G dye on mesoporous activated carbon prepared from Algerian date pits using experimental designs, Desalin. Water Treat. 45 (2012) 284–290.
[7] K.Y. Foo, B.H. Hameed, Recent developments in the preparation and regeneration of activated carbons by microwaves, Adv. Colloid Interface Sci. 149 (2009) 19–27.
[8] A. Rodriguez, G. Ovejero, M. Mestanza, J. Garcia, Dyes adsorption on low cost adsorbents: Inorganic materials, Desalin. Water Treat. 45 (2012) 191–205.
[9] Y.L. Liu, D. Ma, J.L. Li, X.R. Zhao, R.P. Han, Characterization of bio-char from pyrolysis of wheat straw and its evaluation on methylene blue adsorption, Desalin. Water Treat. 46 (2012) 115–123.
[10] V. Mishra, C. Balomajumde, V.K. Agarwal, Sorption of Zn(II) ion onto the surface of activated carbon derived from eucalyptus bark saw dust from industrial wastewater: Isotherm, kinetics, mechanistic modeling, and thermodynamics, Desalin. Water Treat. 46 (2012) 332–351.
[11] J.Q. Liang, J.H. Wu, P. Li, X.D. Wang, B. Yang, Shaddock peel as a novel low-cost adsorbent for removal of methylene blue from dye wastewater, Desalin. Water Treat. 39 (2012) 70–75.
[12] F.C.C. Assis, S. Albeniz, A. Gil, S.A. Korili, R. Trujillano, M. A. Vicente, L. Marcal, M. Saltarelli, K.J. Ciuffi, Removal of organic pollutants from industrial wastewater: Performance evaluation of inorganic adsorbents based on pillared clays, Desalin. Water Treat. 39 (2012) 316–322.
[13] L. Torkian, B.G. Ashtian, E. Amereh, N. Mohammadi, Adsorption of Congo red onto mesoporous carbon material: Equilibrium and kinetic studies, Desalin. Water Treat. 44 (2012) 118–127.
[14] M.L. Lin, Z.W. Zhao, F.Y. Cui, S.J. Xia, Modeling of equilibrium and kinetics of chlorobenzene (CB) adsorption onto powdered activated carbon (PAC) for drinking water treatment, Desalin. Water Treat. 44 (2012) 245–254.
[15] O. Kerkez, S.S. Bayazit, H. Uslu, A comperative study for adsorption of methylene blue from aqueous solutions by two kinds of amberlite resin materials, Desalin. Water Treat. 45 (2012) 206–214.
[16] M.C. Shih, Kinetics of the batch adsorption of methylene blue from aqueous solutions onto rice husk, effect of acid-modified process and dye concentration, Desalin. Water Treat. 37 (2012) 200–214.

[17] Q. Zhou, W.Q. Gong, C.X. Xie, Y.B. Li, C.P. Bai, S.H. Chen, Biosorption of methylene blue from aqueous solution on spent cottonseed hull substrate for *Pleurotus ostreatus* cultivation, Desalin. Water Treat. 29 (2011) 317–325.
[18] A.O. Yasmine, C. Malika, A. Abdeltif, B. Aicha, Sorption of hexavalent chromium metal onto Amberlite IRA 410 – Equilibrium isotherms and kinetic studies, Desalin. Water Treat. 38 (2012) 278–415.
[19] I. Langmuir, The adsorption of gases on plane surfaces of glass, mica and platinum, J. Am. Chem. 57 (1918) 1361–1403.
[20] H. Freundlich, Über die adsorption in lösungen (Adsorption in solution), Z. Phys. Chem. 57 (1906) 384–470.
[21] M.I. Tempkin, V. Pyzhev, Kinetics of ammonia synthesis on promoted iron catalyst, Acta Phys. Chim. USSR 12 (1940) 327–356.
[22] R.P. Han, J.J. Zhang, P. Han, Y.F. Wang, Z.H. Zhao, M.S. Tang, Study of equilibrium, kinetic and thermodynamic parameters about methylene blue adsorption onto natural zeolite, Chem. Eng. J. 145 (2009) 496–504.
[23] H. Chen, J. Zhao, A.G. Zhong, Y.X. Jin, Removal capacity and adsorption mechanism of heat-treated palygorskite clay for methylene blue, Chem. Eng. J. 174 (2011) 143–150.
[24] Q. Liu, Y.M. Zhou, L.Q. Zou, T. Deng, J. Zhang, Y. Sun, X.X. Ruan, P. Zhu, G.R. Qian, Simultaneous wastewater decoloration and fly ash dechlorination during the dye wastewater treatment by municipal solid waste incineration fly ash, Desalin. Water Treat. 32 (2011) 179–186.
[25] T.H. Liu, Y.H. Li, Q.J. Du, J.K. Sun, Y.Q. Jiao, G.M. Yang, Z. H. Wang, Y.Z. Xia, W. Zhang, K.L. Wang, H.W. Zhu, D.H. Wu, Adsorption of methylene blue from aqueous solution by grapheme, Colloids Surf. B 90 (2012) 197–203.
[26] P. Gao, Z.H. Liu, G. Xue, B. Han, M.H. Zhou, Preparation and characterization of activated carbon produced from rice straw by $(NH_4)_2HPO_4$ activation, Bioresour. Technol. 102 (2011) 3645–3648.
[27] K. Nuithitikul, S. Srikhun, S. Hirunpraditkoon, Influences of pyrolysis condition and acid treatment on properties of durian peel-based activated carbon, Bioresour. Technol. 101 (2010) 426–429.
[28] T.H. Wang, S.X. Tan, C.H. Liang, Preparation and characterization of activated carbon from wood via microwave-induced $ZnCl_2$ activation, Carbon 47 (2009) 1867–1885.
[29] X.H. Xue, X.S. He, Y.H. Zhao, Adsorptive properties of acid-heat activated rectorite for Rhodamine B removal, equilibrium, kinetics studies, Desalin. Water Treat. 37 (2012) 259–267.
[30] S. Lagergren, Zur theorie der sogenannten adsorption geloster stoffe, Kungliga Svenska Vetenskapsakademiens [About the theory of so-called adsorption of soluble substances, Kungliga Svenska Vetenskapsakademiens]. Handlingar 24 (1898) 1–39.
[31] Y.S. Ho, Adsorption of heavy metals from waste streams by peat, PhD Thesis, University of Birmingham, Birmingham, UK, 1995.
[32] L. Tian, G. Xie, R.X. Li, X.H. Yu, Y.Q. Hou, Removal of Cr (VI) from aqueous solution using MCM-41, Desalin. Water Treat. 36 (2011) 334–343.
[33] F. Deniz, S.D. Saygideger, Equilibrium, kinetic and thermodynamic studies of Acid Orange 52 dye biosorption by *Paulownia tomentosa* Steud. Leaf powder as a low-cost natural biosorbent, Bioresour. Technol. 101 (2010) 5137–5143.
[34] W.J. Weber, J.C. Morris, Kinetics of adsorption on carbon from solution, J. Sanitary Eng. Div. Proc. Am. Soc. Civ. Eng. 89 (1963) 31–59.
[35] V.J.P. Poots, G. McKay, J.J. Healy, The removal of acid dye from effluent using natural adsorbents: I. Peat, Water Res. 10 (1976) 1061–1066.
[36] W.H. Cheung, Y.S. Szeto, G. McKay, Intraparticle diffusion processes during acid dye adsorption onto chitosan, Bioresour. Technol. 98 (2007) 2897–2904.